BULLETIN OF THE POLISH ACADEMY OF SCIENCES
TECHNICAL SCIENCES, Vol. 72(4), 2024, Article number: e150108
DOI: 10.24425/bpasts.2024.150108

Development of high-temperature permanent magnet synchronous motor for autonomous robotic navigation: a design and finite element analysis approach

Anand M*, Sundaram M, Sivakumar P, and Angamuthu A

Department of Electrical and Electronics Engineering, PSG College of Technology, Tamilnadu, India

Abstract. Traditional industrial robots come with prime movers, i.e. electric motors (EMs), which range from a few hundred to just a few kilo watts of power ratings. However, for autonomous robotic navigation systems, we require motors which are lightweight with the aspect of high torque and power density. This aspect is very critical when the EMs in robotic navigations are subjected to harsh high temperature survival conditions, where the sustainability of the performance metrics of the electromagnetic system of the EMs degrades with the prevailing high temperature conditions. Hence, this research work addresses and formulates the design methodology to develop a 630 W high temperature PMSM (HTPMSM) in the aspect of high torque and power density, which can be used for the autonomous robotic navigation systems under high temperature survival conditions of 200°C. Two types of rotor configurations i.e. the surface permanent magnet type (SPM) and the interior permanent magnet type (IPM) of HTPMSM are examined for its optimal electromagnetic metrics under the temperature conditions of 200°C. The 630 W HTPMSM is designed to deliver the rated torque of 2 Nm within the volumetric & diametric constraints of DxL, which comes at 80×70 mm at the rated speed of 3 000 rpm with the survival temperature of 200°C and target efficiency greater than 90%. The FEM based results are validated through the hardware prototypes for both SPM and IPM types, and the results confirm the effectiveness of the proposed design methodology of HTPMSM for sustainable autonomous robotic navigation applications.

Keywords: permanent magnet synchronous motor (PMSM); high temperature; torque density; power density; efficiency.

1. INTRODUCTION

EMs are the main prime movers for industrial robots which are designed for their optimal electromagnetic characteristics for various classes of duty cycles. The power ratings of traditional industrial robots vary from a few hundred to just a few kilo watts. The EM in these robots can deliver the rated torque at optimally loaded conditions. Due to the widespread applications of robots, miniature robots which are highly essential for the autonomous navigation systems are becoming more popular due to their light weight, compactness and effectiveness in control of the applications related to humanoid robots. These lightweight robots are nowadays of paramount importance, since they find versatile application in high temperature fields such as the chemical, petroleum, aerospace, mineral mining, oil exploration, robotic exploration systems and non-destructive testing vehicle industries due to the advancements in power electronics and robotic control systems [1–7]. The EM used in these miniature robots demands a high torque and power density, since the EM of this robots comes with predefined geometrical and volumetric constraints. The challenging task of the EM in these types of miniature robots is their sustainability in survival during autonomous navigation under high temperature conditions, as the resistances of the EM increase with increase in temperature, which yield reduction in the operating efficiency and hence the yielded torque.

Among the different types of EM, which include induction, synchronous reluctance, switched reluctance and permanent magnet motors, the PMSM based servo motors find widespread usage in robotic navigations, due to their higher torque and higher power density, which is satisfied by the usage of permanent magnetic materials, and which renders the system lightweight, an ideal factor for miniature robots. This is a crucial factor for the autonomous robotic exploration systems, since the robots which are steered by its electric actuators demand a constant torque and less vibration with an extended speed range to become sustainable even under harsh temperature conditions. However, permanent magnets are confined to the effect of magnetic saturation under elevated temperature levels, which account for the limiting factor in the designer's choice of PMSM for high temperature applications.

Improvements in the performance metrics of the BLDC motor for high temperature applications were discussed in [8]. The BLDC motor being considered is driving the fuel pump of a combat vehicle. The work concentrates on solving the issue of stator slip of the BLDC motor which occurs due to elevated temperatures of the combat vehicle. The investigation of the

*e-mail: and.eee@psgtech.ac.in

Manuscript submitted 2023-02-06, revised 2024-03-07, initially accepted for publication 2024-03-13, published in July 2024.

performance characteristics of various materials of an IPM machine for a traction application under variations in temperatures is presented in [9]. The motor peak power considered is 105 kW and the paper presents the fundamentals of effect of temperature on an IPM machine performance metrics such as the speed-torque curve, constant torque curve, voltage limit ellipses and maximum torque per ampere curves.

The design of a 12 kW PMSM for a wide temperature range, ranging from −60°C to 300°C for a rotational speed of 12 krpm with a targeted efficiency of 90% was reported in [10]. The selection and performance metrics of the hard and soft magnetic materials at the elevated temperatures has also been briefly described. In [11], the thermal investigation of a SPM type of PMSM designed for aerospace actuation applications for the elevated temperature levels of 200°C is presented. The paper lays down the thermal computational process in the analysis of PMSM and the test results validate the effectiveness of the proposed design methodology, as compared to FE analysis.

The IPM type of motor for traction applications, designed with the aspect of higher power density to meet the specifications of FreedomCAR 2020, was discussed in [12]. The continuous power rating of the motor is 30 kW, with the minimum top speed of 14 000 rpm at an efficiency of > 95%. The ambient operating temperature of the motor is −40°C to 140°C. The paper concludes with the various performance metrics that have to be evaluated at the elevated operating temperature conditions. In [13], the effect of magnetic material grades at high temperatures on the performance of an IPM type machine for electric vehicle application was presented. The motor has a power rating of 55 kW, with 2 000 rpm as the minimum speed in the constant torque region of operation. 5 different variants of NdFeB magnets such as HS_43EH, HS_40FH, HS_36EH, HS_32GH and HS_35EH are considered with various operating temperature limits. The study investigates and come to conclusion concerning the various performance metrics for the temperature dependent material characteristics of the IPM at high temperatures.

In [14], the effect of temperature on the performance of a ferrite-based PMBLDC motor of 700 W, which is intended to be used for electric 2-wheeler application at the maximum speed of 32 km/h, was discussed. The study proves that the performance of the motor varies beyond the constant torque operation due to the influence of the temperature on the magnets, and the authors urge the motor designer to ensure the irreversible demagnetization characteristics of the ferrite magnets under such temperature variations.

2. RESEARCH QUESTIONS

A detailed literature survey has been discussed in the section above, concentrating on the design of miniature robotic motors for high temperature operating conditions. Though several high temperature motors are examined and investigated in the literature for higher power ratings, where there is an opportunity for optimization for the volumetric and diametric length, research on miniature EM for the navigation robots for harsh temperature conditions is not available yet. The critical constraint for the EM in these robots is that they come with the defined volumetric & diametric constraints (DxL) due to the space and weight metrics of the robotic navigation systems. Also, based on the literature study, it is found that there is lack of systematic methodology for the design of electric actuators for miniature robotic vehicles under elevated temperatures. There is a research gap identified, which makes the authors concentrate on developing a PMSM as an electric actuator for these types of miniature robots with higher power and torque density metrics. The outcomes of this research will be useful to the research community who are working on the EM in robotic navigation systems to be used under harsh temperature conditions.

The research work presented here provides a substantial view and answers the below-mentioned research questions.

1. Whether the PMSMs are suited for harsh temperature survival conditions?
2. Whether the PMSMs can deliver higher power and torque density metrics at elevated temperature within the defined frame size?
3. What type of PMSM (SPM or IPM) will deliver constant torque characteristics under harsh temperature conditions?
4. What type of materials do we need for the PMSM at elevated temperature conditions?
5. Whether the designed PMSM shall be efficient at higher temperature?

3. DESIGN METHODOLOGY FOR HTPMSM

The design methodology involved in the design of HTPMSM is depicted in the flowchart shown in Fig. 1 with consideration of optimal electromagnetic characteristics [15, 16]. The major dimensional metrics such as D and L which determine the volumetric and diametric sizing of the HTPMSM are calculated from equations (1)–(3) [16].

$$P = T_{\text{RotorVolume}} \cdot V_r \cdot \frac{2\pi N}{60}, \tag{1}$$

$$D^2 L = (P \cdot 4 \cdot 60) / \left(2\pi^2 \cdot T_{\text{RotorVolme}} \cdot N\right), \tag{2}$$

$$P = T_{\text{RotorVolume}} \cdot \frac{\pi D^2 L}{4} \cdot \frac{2\pi N}{60}, \tag{3}$$

where:
P – rated power of the HTPMSM (kW),
$T_{\text{RotorVolume}}$ – torque per rotor volume of HTPMSM (kNm/m^3),
V_r – rotor volume of HTPMSM (m^3),
N — rated speed of HTPMSM (rpm),
D – inner diameter of the stator of HTPMSM (mm),
L – stack length of the core of HTPMSM (mm).

The torque per rotor volume of HTPMSM with the sized metrics of D and L are validated using equation (4) which gives the relationship between electric loading, magnetic loading and the torque per rotor volume [16].

$$T_{\text{RotorVolume}} = \frac{\pi}{\sqrt{2}} \cdot K_w \cdot A \cdot B, \tag{4}$$

where:
A – specific electric loading of HTPMSM (ampere/m),
B – specific magnetic loading of HTPMSM (Wb),
K_w – winding factor of HTPMSM.

The electric loading (A) is defined by the ratio of total ampere conductors to the circumference of the airgap as defined by equation (5).

$$A = \frac{2m \times T_{ph} \times I_{ph}}{\pi D}, \tag{5}$$

where:
m – number of phases of HTPMSM,
T_{ph} – turns/phase of HTPMSM,
I_{ph} – phase current of HTPMSM (ampere).

The magnetic loading (B) is related to the fundamental flux/pole of HTPMSM as defined by equation (6).

$$\Phi_1 = B \cdot \frac{\pi \cdot D \cdot L}{p}, \tag{6}$$

where:
Φ_1 – fundamental flux/pole of HTPMSM (Wb),
p – number of pole pairs.

The turns/phase of HTPMSM is governed by equation (7), taking consideration of the fundamental flux/pole, fundamental frequency and the fundamental winding factor.

$$T_{ph} = \frac{E}{4.44 k_{w1} \emptyset_1 f}, \tag{7}$$

where:
E – EMF generated/phase (V),
k_{w1} – fundamental winding factor,
f – fundamental frequency (Hz).

The air-gap length of HTPMSM is defined by equation (8), which relates the air-gap reluctance, permittivity of free space and the air-gap area for the defined stator and rotor geometries.

$$R_g = \frac{g}{\mu_0 A_g}, \tag{8}$$

where:
g – air-gap length (m),
R_g – reluctance of the air-gap (AT/Wb),
μ_0 – permittivity of free space ($4\pi \times 10^{-7}$ H/m),
A_g – area of the air-gap (m^2).

The slot geometrical dimensions and area are fixed as per the design formulations listed in the design flowchart in Fig. 1. The performance metrics of the permanent magnet used in HTPMSM are of paramount importance, since at elevated temperatures the HTPMSM magnet must not be subjected to demagnetization. Also, the magnetic design equations compute the optimal flux density from these permanent magnets, which are designed as per the load line plot under the elevated temperature conditions for the optimal loading of HTPMSM.

The permeance coefficient of the HTPMSM magnet (P.C.), which is defined as the parameter used to identify the optimal operating point for the given magnet on its B-H curve, is defined

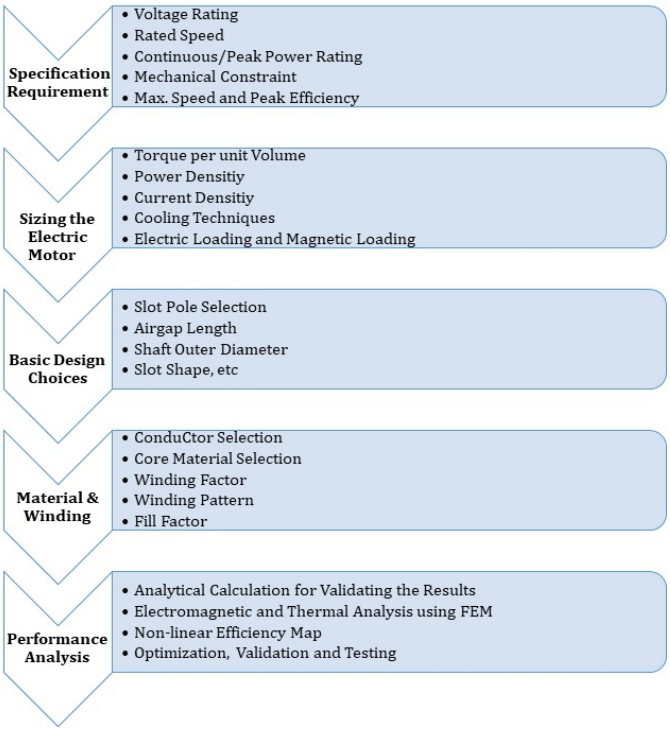

Fig. 1. Design methodology of HTPMSM

by equation (9).

$$\text{P.C.} = B_m / H_m, \tag{9}$$

where:
P.C. – permeance coefficient of the HTPMSM magnet,
B_m – magnetic flux density of HTPMSM (Wb/m^2),
H_m – magnetizing force of HTPMSM (A/m).

The magnetic flux density and magnetizing force of HTPMSM are governed by equations (10) and (11), respectively.

$$B_m = \frac{B_g \cdot A_g}{A_m}, \tag{10}$$

$$H_m = \frac{B_g \cdot L_g}{L_m}, \tag{11}$$

where:
B_g – air-gap flux density (T),
A_g – area of the air-gap of HTPMSM (m^2),
A_m – area of the HTPMSM magnet (m^2),
L_g – length of the air-gap of HTPMSM (m),
L_m – length of the HTPMSM magnet (m).

The area of the air-gap and the magnet area of HTPMSM are governed by equations (12) and (13), respectively.

$$A_g = \pi \cdot \frac{D \cdot L}{2}, \tag{12}$$

$$A_m = \pi \cdot L \times \frac{120}{180} \cdot \frac{(D - L_m)}{2}. \tag{13}$$

By substituting equations (10)–(13) in equation (9), the value of the permeance coefficient is arrived at, as shown in equa-

tion (14).

$$\text{P.C.} = \left(\frac{A_g}{A_m}\right) \cdot \left(\frac{L_m}{L_g}\right). \tag{14}$$

The P.C. is used to determine the demagnetization characteristics of the permanent magnetic grade under the high temperature conditions by sketching its load line plot. This will ensure the optimal energy product of the permanent magnet of HTPMSM from which the size metrics of the magnet shall be arrived at, as per the specific magnetic loading design formulations depicted in the electromagnetic design flowchart of HTPMSM, as shown in Fig. 1.

4. FEM ANALYSIS AND PERFORMANCE METRICS OF HTPMSM SPM TYPE

The research work starts with the objective of design and development of a high-temperature PMSM to survive at an ambient temperature of 200°C and to meet the performance metrics required as specified in Table 1. The conceptual design of HTPMSM is first evaluated for the surface permanent magnet rotor type. It is necessary to identify and classify the conceptual functionality of the components design at high temperature operation to perform the required analysis. From the electric machine design aspect, it can be classified as a stationary component and rotating components. The primary function of stator design includes magnetics and electrical factors, yet its secondary function includes the mechanical aspect. Table 2 illustrates the conceptual functionality of the components in an electric motor and hence a requirement for analysis is identified.

Table 1
Design specifications

Parameter	Value
Rated torque	2 Nm
Rated speed	3 000 rpm
DC bus voltage	300 Volts
Magnet type	samarium cobalt
Ambient temperature	200°C
Duty cycle	S8
Frame length	180 mm
Shaft diameter	12.5 mm
Shaft length	32 mm

Table 2
Conceptual functionality of HTPMSM components

Magnetic design	Mechanical design	Electrical design
Rotor lamination	Shaft	Stator coil winding
Stator lamination	Housing & end cap	Slot liner insulation
Rotor magnets	Lamination for creep stress	Wedge
Retaining sleeves	Bearings	Coil separator

The main source of heat is due to the ambient temperature from the exterior of the motor environment and hence the current method of approach involves materials in the housing and shaft to isolate/shield from this environment and to enable to match the thermal coefficient of materials at steady state. Additionally, due to I^2R loss that occurs as joules, heat loss in the stator winding is attributed and extended towards the operation of high temperature environment conditions, which introduces challenges to materials design used in the electric motor. These challenges include diffusional process and hence variation of microstructure of the electrical, magnetic components, and require careful consideration of the following key metrics for optimal loaded conditions.

- Inter-laminar insulation in magnetic materials.
- Insulation of wires for stator coils.
- Stator, rotor and shaft materials for stress analysis.
- Mismatches in coefficients of thermal expansions of components.

Considering the magnetic saturation at high temperature, Hiperco 50/ Vacodur 50 is used for stator and rotor lamination. Inconel 600 is used for shaft material, considering the thermal expansion and strength of material at high temperature. Table 3 shows the key materials selected for the design of HTPMSM SPM type and FEM analysis is performed. The summary of the design parameters involved in HTPMSM SPM type electric machine design is presented in Table 4.

Table 3
Materials for HTPMSM components

Component	Materials
Shaft	Inconel 600
Stator & rotor laminations	Hiperco 50/ Vacodur 50
Magnet grade	R 33E- Recoma Sm2Co17
Rotor retaining sleeves	Hastelloy N, Nickel 200
Wire winding & insulation	Ceramic coated Cu

Table 4
Design parameters of HTPMSM SPM type

Parameter	Value	Unit
Outer rotor diameter	50	mm
Rated speed	3 000	rpm
Continuous torque	2	Nm
No. of poles	10	#
Stator outer diameter	82.5	mm
Continuous power rating	630	W
Air-gap length	1	mm
Working temperature	200	°C
Stack length	90	mm
Magnet thickness	3	mm

The slot/pole combination of the HTPMSM SPM type is decided based on the optimal electromagnetic factors [17, 18]. The number of stator slots is selected as 12 and the number of rotor poles is selected as 10 to yield an optimized electromagnetic circuit as shown in Fig. 2a. FEM analysis is carried out through the software Motorsolve electromagnetic solver under the defined ambient temperature condition of 200°C. Instantaneous magnetic flux density is depicted in Fig. 2b, which shows that the HTPMSM SPM type machine configuration is well within the permissible limits, as depicted from the guideline values of the flux density listed in Table 5 for the ambient temperature condition of 200°C.

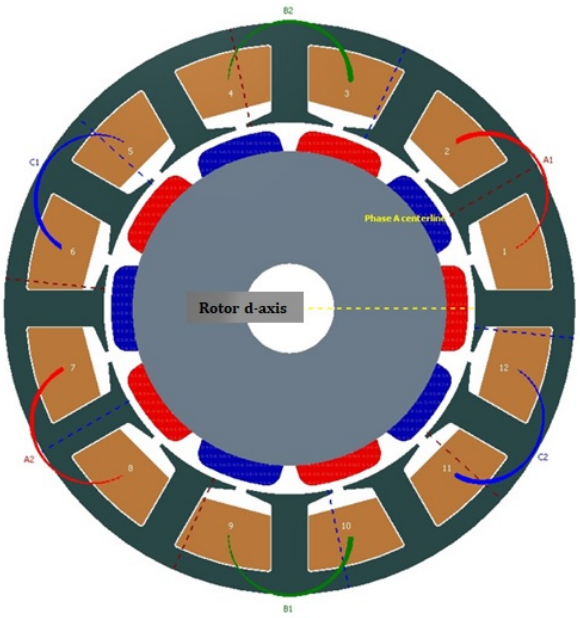

(a) Stator and rotor configuration

Table 5
Flux density points of HTPMSM

Flux density points	Value
Stator tooth	1.80 T
Airgap	0.60 T
Rotor yoke	1.68 T
Stator yoke	1.1 T

BEMF of the HTPMSM SPM type is shown in Fig. 3. It is observed that BEMF is sinusoidal in nature, which prevents the motor from making a noise and vibrating under dynamic loaded conditions. Also, the current ripple is less similar to the one depicted in Fig. 4, since hysteresis current control band is applied to HTPMSM to minimize the current ripple for an efficient PMSM design at the rated conditions. The current reference as shown in Fig. 4 corresponds to the phase current of HTPMSM SPM type rotor configuration. As observed from Fig. 4, the current doesn't reach the lower and upper reference limits in the

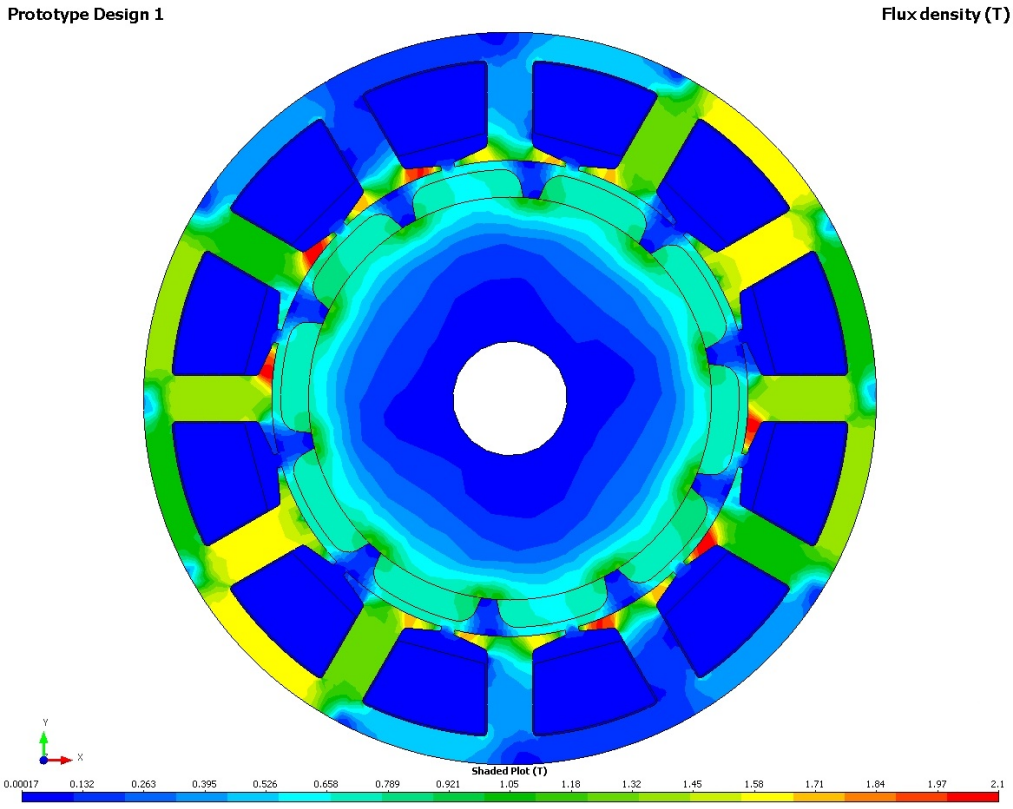

(b) Instantaneous flux density

Fig. 2. HTPMSM SPM type: spatial plots

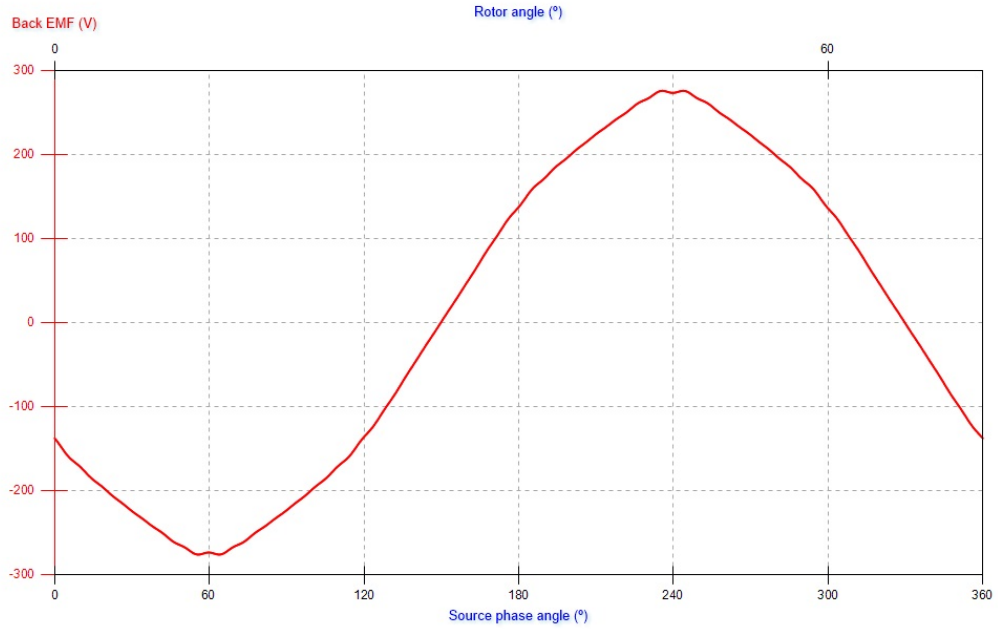

Fig. 3. HTPMSM SPM type: back EMF @ 3 000 rpm

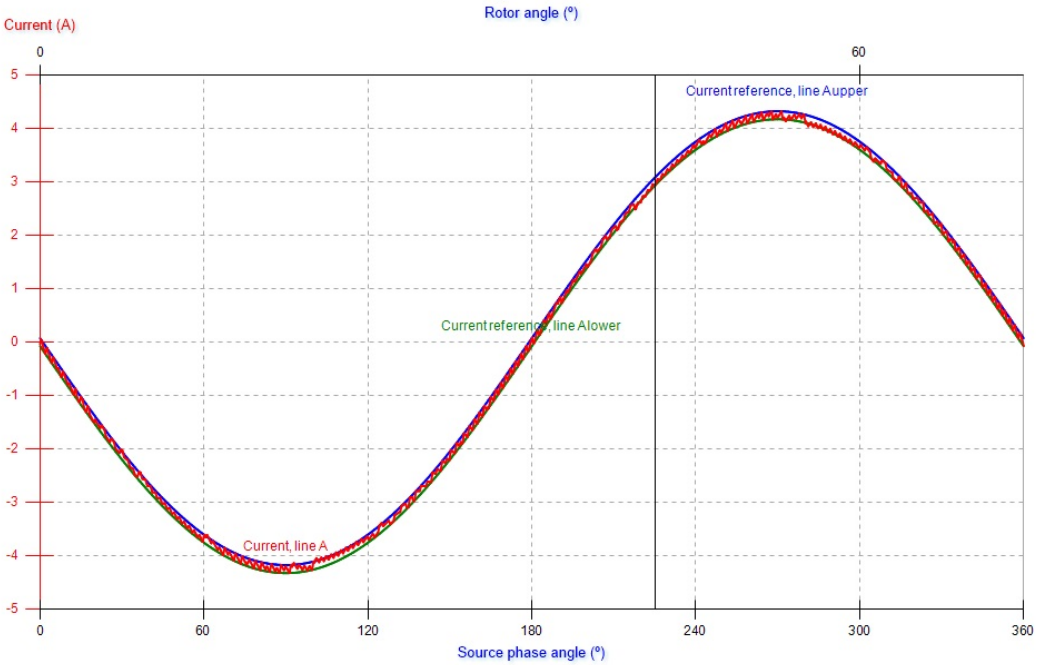

Fig. 4. HTPMSM SPM type: phase current

lower half and upper half of the wave symmetry even though hysteresis current band controller is used, and it is also observed that this happens for a marginal or limited duration of the source phase angle and in major time durations, and the hysteresis current band controller tries to maintain the slope (both positive and negative slopes) of the actual current within the band reference limits of the hysteresis current band controller. The reasons for these variations shall be attributed to non-linear change in the slope of the actual current when it reaches the lower and upper wave extremes, which is predominantly due to the non-linearity of the magnetic forces due to circumferential rotation, mechanical stresses and partial unbalanced magnetic pull under elevated temperature conditions and as a result, the required gain to tune the controller in the vector control strategy is momentarily lapsed for a marginal or limited duration, making the current not reach the upper and lower limits of reference values as dictated by the hysteresis current band controller. For the aforementioned reasons as evident by the broken samples

of HTPMSM SPM type rotor magnets, depicted in Fig. 7, the IPM rotor configuration of HTPMSM as shown in Fig. 8a is proposed.

The speed-torque characteristics of the HTPMSM SPM type is shown in Fig. 5 at the ambient temperature condition of 200°C. From Fig. 5, it is inferred that the HTPMSM SPM type is delivering a constant torque characteristic till the base speed of 3 000 rpm, beyond which field a weakening region is achieved for the ambient temperature condition of 200°C. Also, from the thermal fields as depicted from the thermal field plot shown in Fig. 6, the designed motor is well within the permissible limits of the elevated temperatures of 200°C [19].

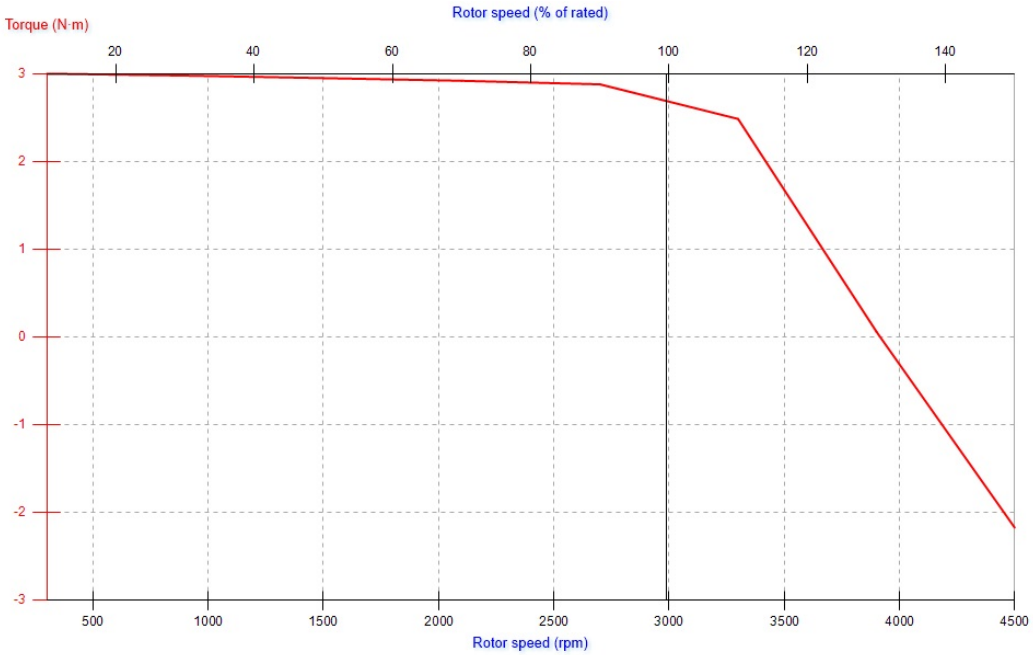

Fig. 5. HTPMSM SPM type: speed – torque characteristics

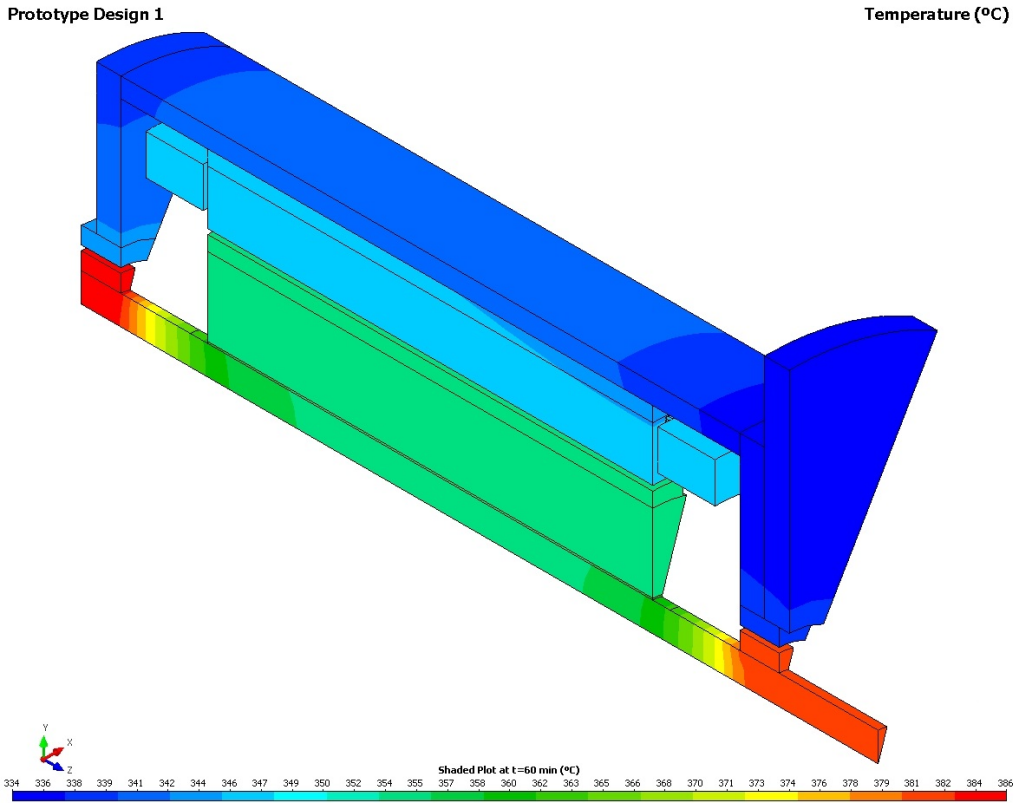

Fig. 6. HTPMSM SPM type: thermal fields

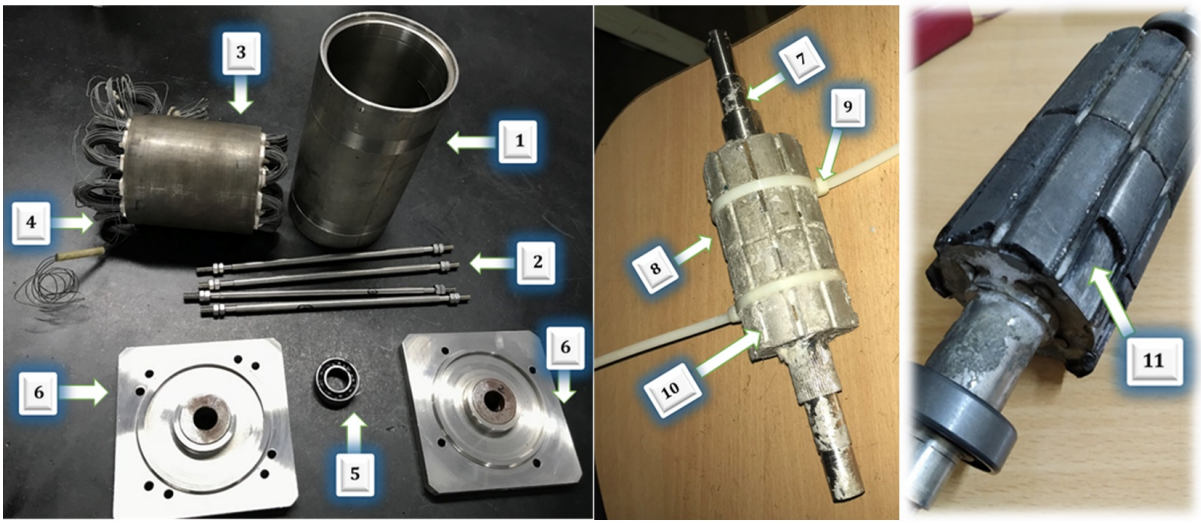

(a) Housing parts (b) Rotor parts (c) Rotor magnets of SPM

1. Inconel stator housing, 2. Studs, 3. Vanadium cobalt iron laminations for stator, 4. Stator core with ceramic coated winding, 5. Nichrome coated bearings, 6. Front & back flange mount inconel, 7. Inconel shaft, 8. Recoma grade samarium cobalt magnet, 9. Cable tie, 10. High temperature adhesives – Aremco, 11. Breakdown of rotor magnets

Fig. 7. HTPMSM: SPM type: rotor with housing

The housing parts of the HTPMSM SPM type are shown in Fig. 7a and the rotor with its material description is depicted in Fig. 7b. The fabricated motor is tested with commercial drive under the flux sensorless control methodology. The motor was tested at 1 500 rpm and beyond 1 500 rpm the motor experienced a high level of vibrations. It can be seen from the Fig. 7c that rotor magnets broke partially due to circumferential rotation. However, the magnets were replaced with a new magnet and testing was pursued. Considering any such problems, fault tolerant and reliable rotor configurations at elevated temperatures, a 2nd prototype with the spoke type and magnets inserted in a stack of steel is designed and fabricated.

5. FEM ANALYSIS AND PERFORMANCE METRICS OF HTPMSM IPM TYPE

The spoke type configurations of 12 slots/10 pole is realized considering this configuration will provide some concentration of flux density relatively compared with a surface mounted permanent magnet rotor, and that it will offer fault tolerant capability unlike the HTPMSM SPM type rotor, which encountered broken magnets during the testing. Hence, the spoke type configurations also facilitate higher flux density in the air-gap delivering maximum torque. The summary of the design parameters involved in the HTPMSM IPM type electric machine design is given in Table 6. The number of stator slots and the number of rotor poles are the same as in the HTPMSM SPM type machine configuration shown in Fig. 8a. FEM analysis is carried out under the defined temperature conditions. Instantaneous magnetic flux density is depicted in Fig. 8b, which shows that the HTPMSM IPM type machine configuration is well within the permissible limits as depicted from the flux density guideline values listed in Table 5.

BEMF of the HTPMSM IPM type is shown in Fig. 9. It is observed that BEMF is sinusoidal in nature. Also, the current ripple is less as the one depicted in Fig. 10, since the hysteresis current control band is applied for HTPMSM to minimize the current ripple at the rated conditions.

As inferred from Fig. 10, the measured current of the HTPMSM IPM type reaches the defined lower and upper reference limits of the reference current as dictated by the hysteresis current band controller, thereby yielding an optimised electromagnetic characteristic under elevated temperature conditions. The speed-torque characteristics of the HTPMSM IPM type at the ambient temperature condition of 200°C is shown in Fig. 11.

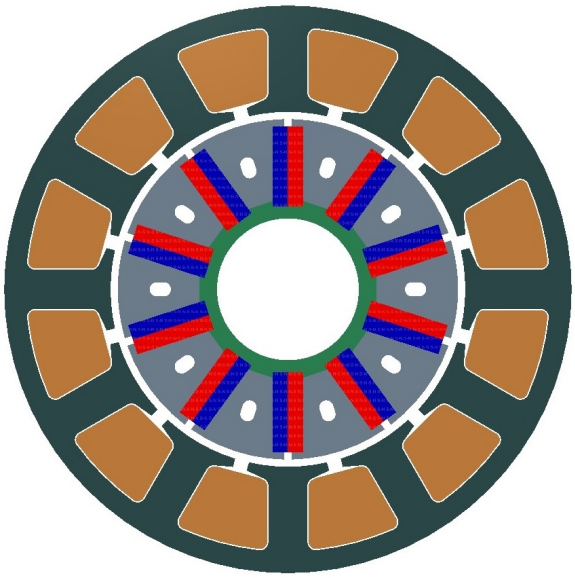

(a) Stator/rotor configuration

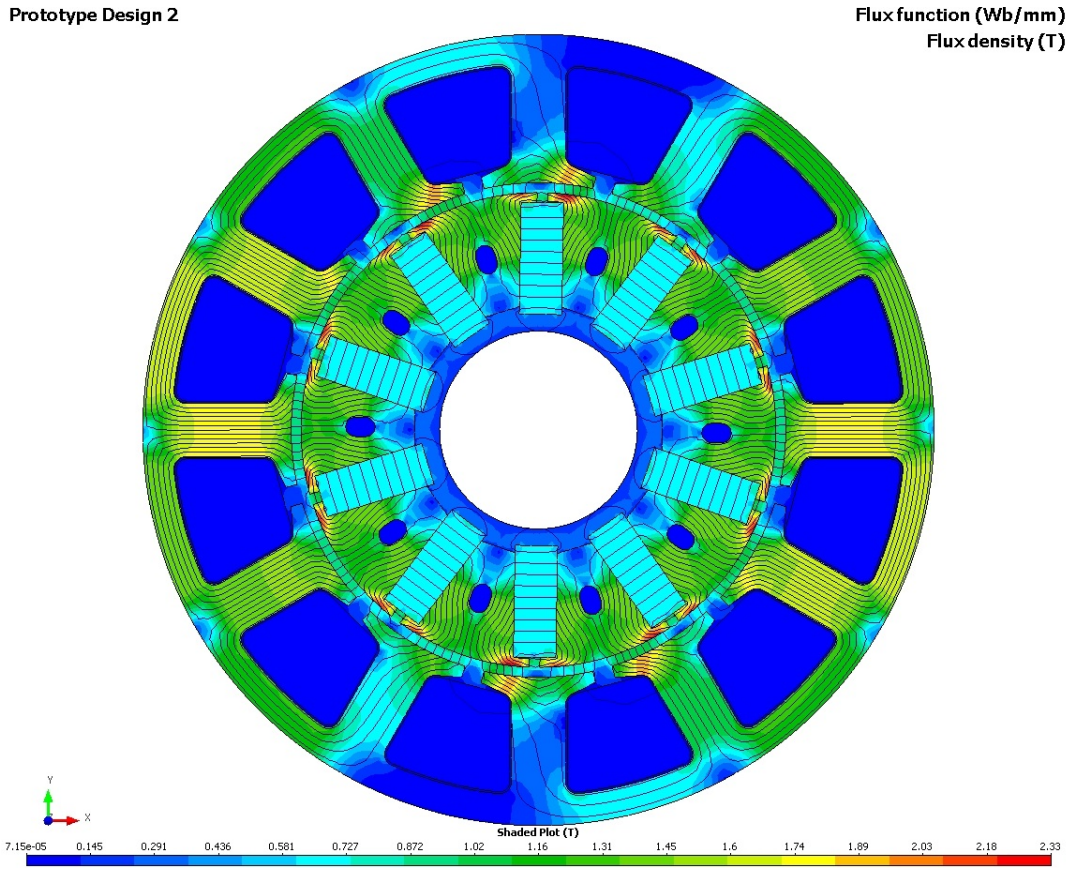

(b) Instantaneous flux density

Fig. 8. HTPMSM IPM Type: spatial plots

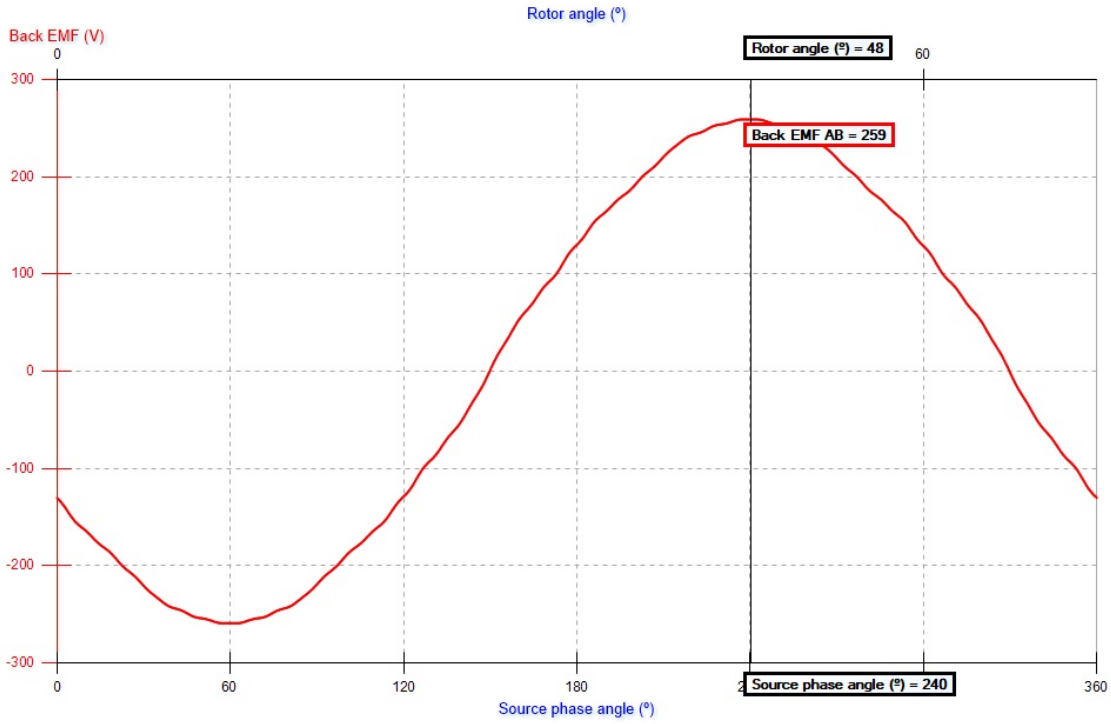

Fig. 9. HTPMSM IPM type: back EMF @ 3 000 rpm

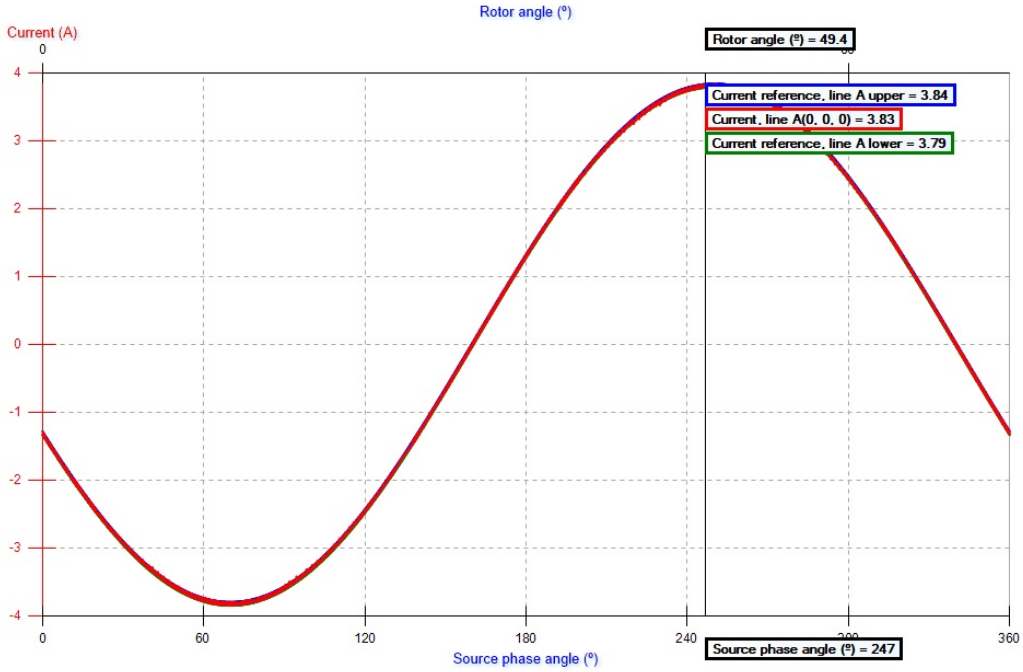

Fig. 10. HTPMSM IPM type: phase current

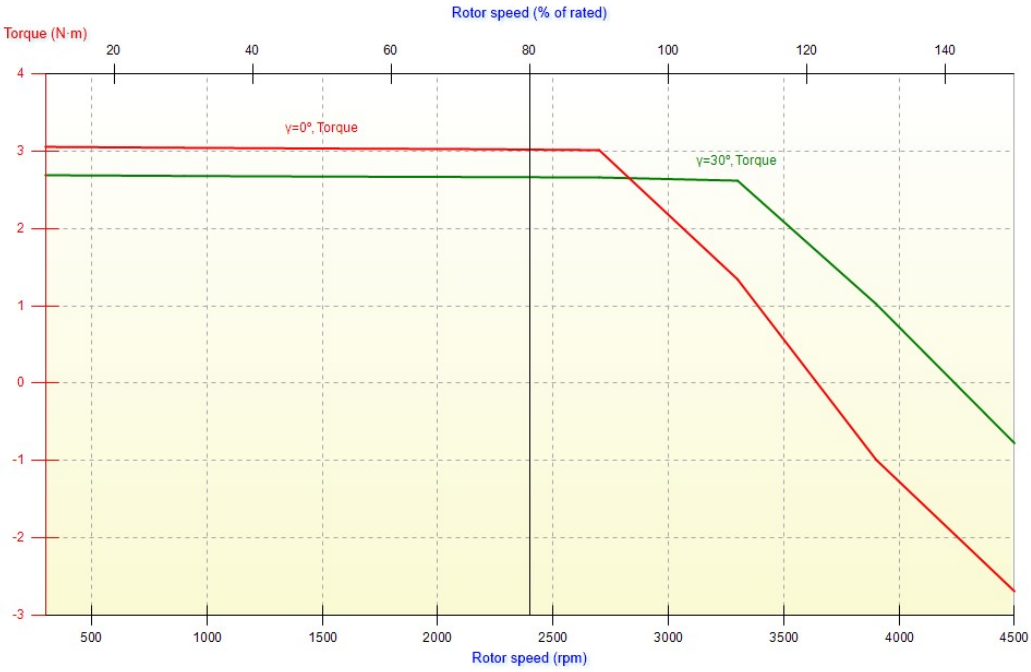

Fig. 11. HTPMSM IPM type: speed – torque characteristics

From Fig. 11, it is inferred that the HTPMSM IPM type is delivering a constant torque characteristic till the rated speed during the FEM analysis carried out at the ambient temperature condition of 200°C.

The designed HTPMSM is required to deliver optimal constant torque from 0 rpm to 3 000 rpm beyond which it shall deliver the variable torque characteristics. From Fig. 11, it is inferred that two different types of Speed Vs Torque characteristics are yielded by the HTPMSM IPM type rotor machine based on the advance phase angles. The characteristics with advance phase angle (γ) of 0° depict that the HTPMSM IPM type rotor can yield a peak torque of 3.1 Nm, reflecting the constant torque characteristics, however such a characteristic is available only till the shaft speed of 2 750 rpm, which is not the desired

Table 6
Design parameters of HTPMSM IPM type

Parameter	Value	Unit
Outer rotor diameter	48	mm
Rated speed	3 000	rpm
Continuous torque	2	Nm
No. of poles	10	#
Stack length (Lstk)	70	mm
Continuous power rating	630	W
Air-gap length	1	mm
Working temperature	200	°C
Stator outer diameter	80	mm
Magnet thickness	4.3	mm

one, beyond which HTPMSM enters into the constant power characteristics (i.e. the field weakening region). Hence, the advance phase angle of the source commutation is advanced to the phase angle (γ) of 30°, which yields a peak torque of 2.8 Nm, reflecting the constant torque characteristics, which is available for an extended range until and beyond the base speed of 3 000 rpm, beyond which the HTPMSM enters into the constant power characteristics. The continuous torque rating of 2 Nm, as desired from the electromagnetic design, is available till and beyond the base speed of 3 000 rpm by the advance phase angle (γ) of 30°, which is frozen for the commutation of the HTPMSM IPM type rotor machine.

Also, based on the thermal fields as depicted in Fig. 12, the designed motor is well within the permissible limits of the elevated temperatures of 200°C. The housing parts of the HTPMSM IPM type are the same as for the SPM type, as shown in Fig. 7, and the IPM rotor is depicted in Fig. 13. The HTPMSM IPM type rotor machine is subjected to the BEMF test to ensure that the generated BEMF is sinusoidal in nature. The BEMF test is done by spinning the rotor of HTPMSM at the required rpm through a prime mover while the reflected terminal voltages are recorded using an oscilloscope.

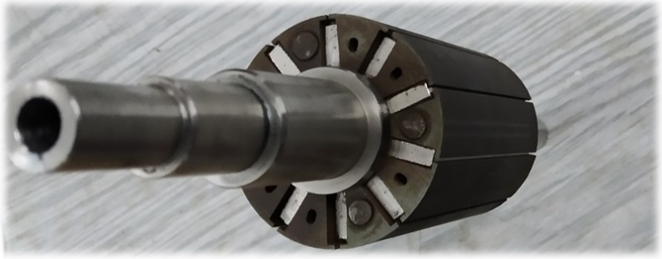

Fig. 13. HTPMSM IPM type: rotor

Figure 14 shows the line-line BEMF observed at the V_{RY}, V_{YB} and V_{BR} lines of HTPMSM, respectively (sinusoidal volt-

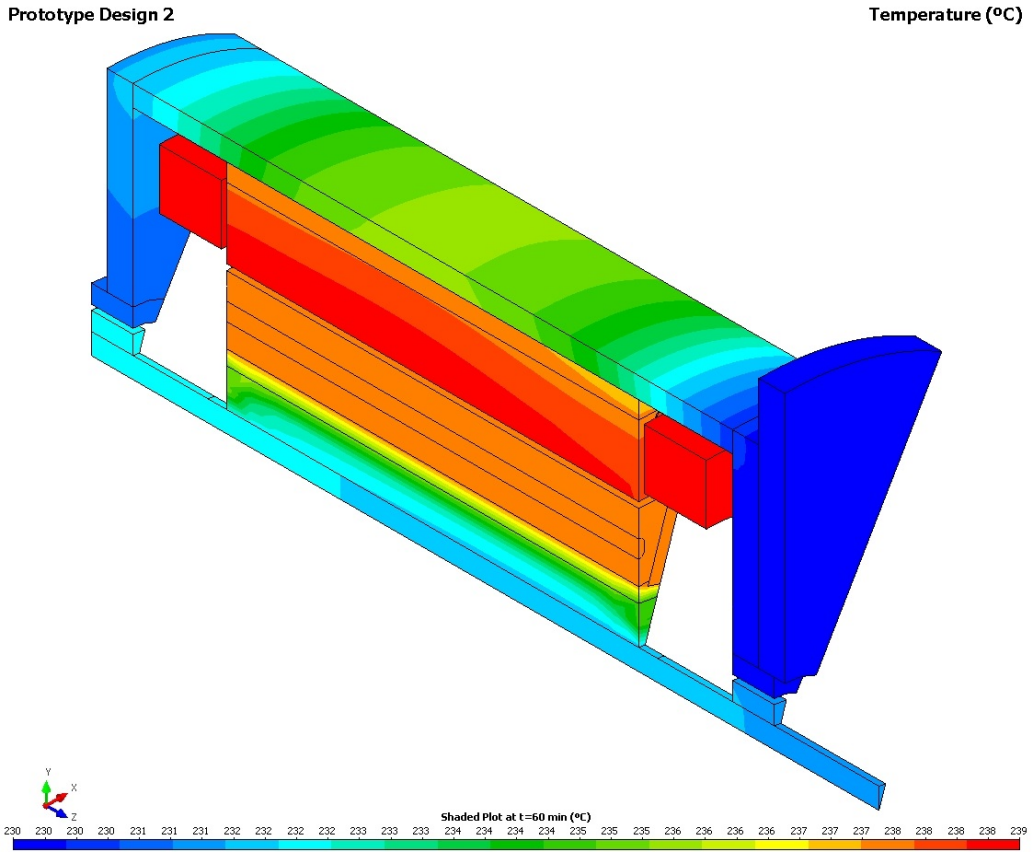

Fig. 12. HTPMSM IPM type: thermal fields

age characteristics), and since the BEMF test is done under no load (no current) conditions of HTPMSM, the line currents are zero as observed from Fig. 14 (zero current characteristics).

It is inferred that BEMF generated by the HTPMSM IPM Type rotor machine is sinusoidal in nature, which validates the effectiveness of the proposed design methodology. This shall be authenticated from the results as shown in Fig. 9. Also, the sinusoidal BEMF characteristics of HTPMSM assure freedom from pulsating spatial harmonics, acoustic noise and vibration, which further enhances the efficiency of HTPMSM under optimally loaded conditions.

The permanent magnet used in the rotor of HTPMSM belongs to the category of samarium cobalt of the sintered Sm2Co17 of the Recoma 33E category. As inferred from equation (14), the P.C. is used to compute the optimal loading point of HTPMSM under the elevated temperature conditions by ensuring a high energy product of HTPMSM as governed by the magnetic design equations formulated from equations (10)–(13). The typical data sheet governing the second quadrant, i.e. the demagnetization characteristics of the sintered Sm2Co17 of the Recoma 33E category as available from the manufacturers data sheet, is depicted in Fig. 17. Using equations (10)–(13), the thickness of the air-gap, the thickness of the magnet and the yielded flux density with defined operating temperature, boundary conditions are computed from the load-line plot as depicted from the Sm2Co17 magnet demagnetization characteristics shown in Fig. 17. This ensures the optimal loading of HTPMSM under the designed high-temperature operating conditions.

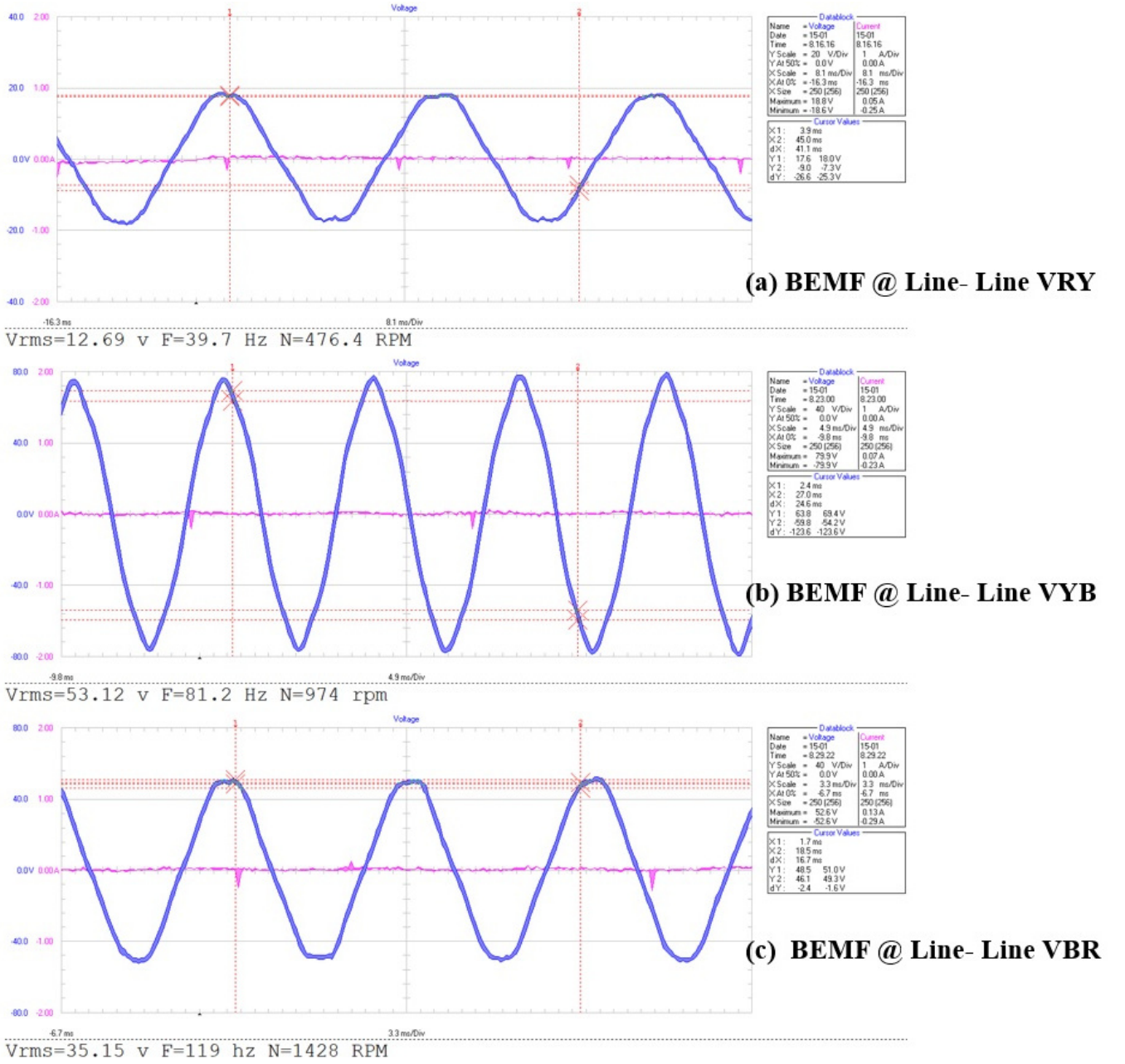

Fig. 14. Line-line BEMF voltages of HTPMSM IPM type rotor

(a) Front flange (b) Frame – top view

Fig. 15. HTPMSM IPM Type – assembled views

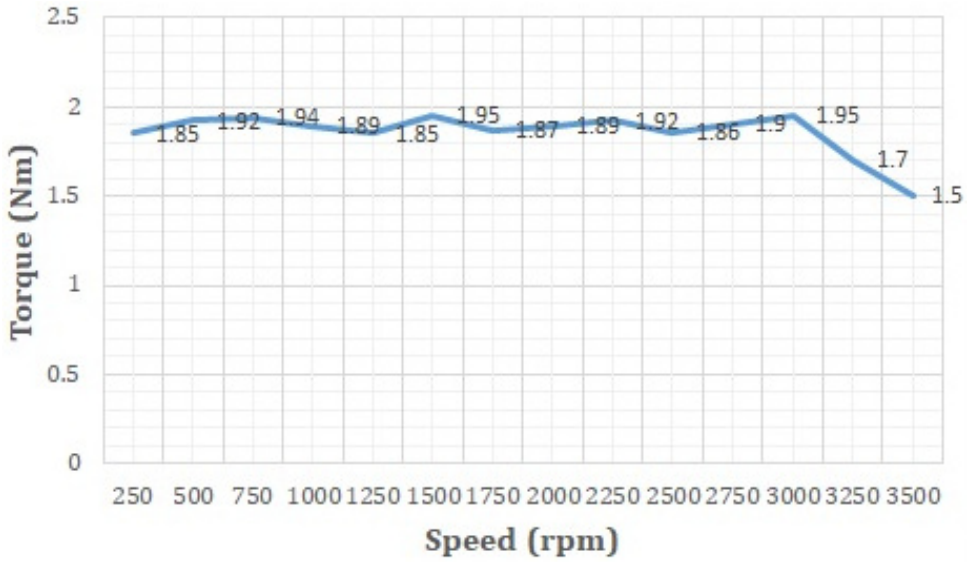

Fig. 16. HTPMSM IPM: speed-torque characteristics at rated loaded conditions

Figure 18 shows the spatial plot representing the remanent flux density of the magnet samples of the HTPMSM IPM rotor. The HTPMSM IPM rotor magnet samples which represent the 10 magnetic poles are placed in the hot chamber and subjected to the hot temperature test. The temperature in the hot chamber is swept from 30°C to 200°C and the remanent flux density of the magnet is observed at the desired test points over the magnetic sample surface using a Gauss meter. The X-axis represents the HTPMSM IPM rotor magnet samples and the Y-axis represents the temperature variation from 30°C to 200°C. The corresponding yielded remanent flux density is pictorially represented by the spatial contour.

It is observed from Fig. 18 that at a lower temperature value of 30°C and at the elevated temperature condition of 200°C, the yielded average flux density of all the HTPMSM IPM rotor magnet samples of 10 numbers stand at 1.15 T and 0.87 T, respectively, which is in correspondence with the desired remanent flux density characteristics of the magnet under consideration, depicted in Fig. 17. The test leads to the conclusion that for a wide band of temperature variation over the HTPMSM IPM rotor magnet samples, there is a minimal variation of the remanent flux density following the magnetic characteristics as depicted in Fig. 17, and hence the proposed magnetic grade is able to yield the required flux density at the elevated temperature conditions of 200°C.

The front flange and the top view of the motor is shown in Fig. 15 and a hot chamber is used for the load test under harsh temperature conditions. The HTPMSM IPM type is powered by a variable frequency drive to test the designed HTPMSM at the ambient high temperature of 200°C for the rated speed-torque

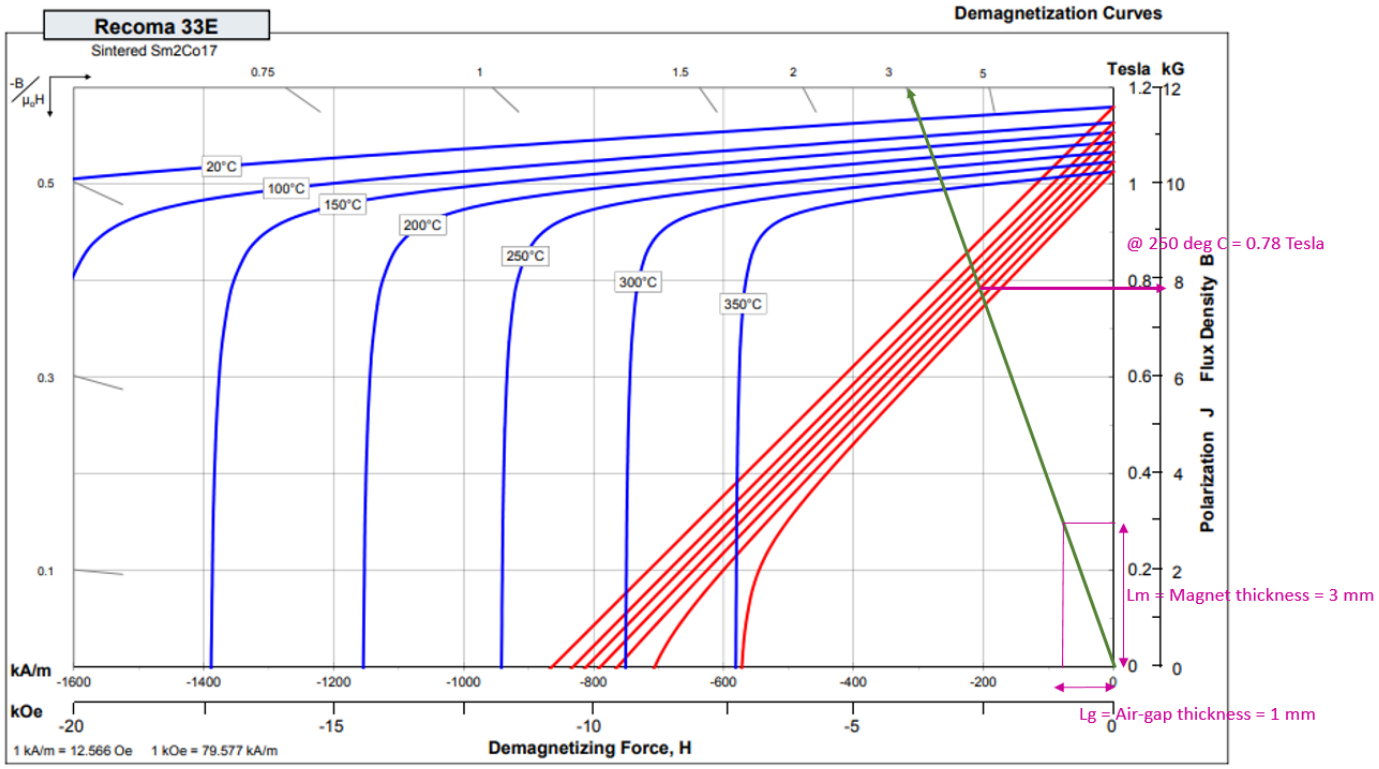

Fig. 17. Demagnetization characteristics of Sm2Co17 magnet

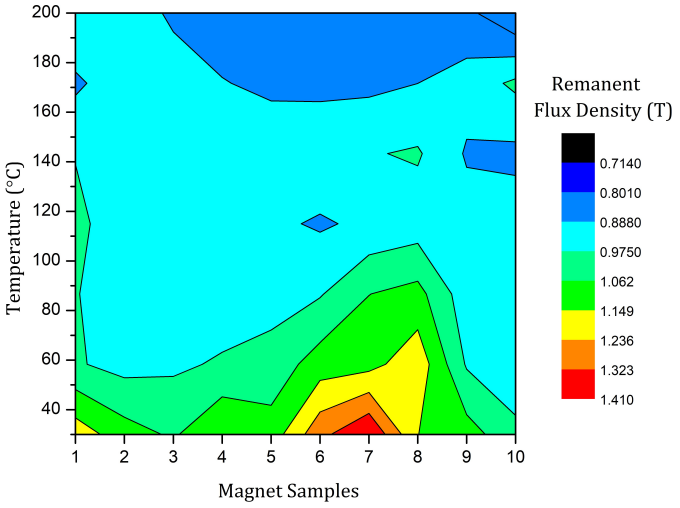

Fig. 18. Spatial plot of remanent flux density of HTPMSM IPM rotor

Table 7
Temperature distribution on HTPMSM IPM type

Time (minutes)	View 1			View 2		
	Max	Avg	Min	Max	Avg	Min
5	35.7	30.2	25.2	30.3	26.5	24.9
10	35.1	29.1	25.7	32.2	27	24.9
15	36.8	28.9	25.1	32.4	27.4	25.1
20	36.5	30.1	26.1	34.1	28.4	25.4
48	36	30.3	26.2	37.4	30.8	26.1

View I: Thermal camera faced towards front view of the motor (front flange)
View II: Thermal camera faced towards top view of the motor (frame – top view)

conditions. Using the Fluke thermal imager, the HTPMSM front flange and frame were monitored for the temperature conditions and recorded with respect to every time instant until 48 minutes for steady state, and the temperature gradients are tabulated in Table 7. The temperature distribution on the surface of the HTPMSM IPM type motor is depicted at a time instant of 5 minutes and its gradients are shown in Fig. 19.

Under no load due to increased resistance, when the motor is operated at ambient temperature of 200°C, the motor draws 0.42 A at 2 300 rpm and at a speed of 3 000 rpm the motor draws 0.55 A. The motor component was able to sustain the ambient temperature as depicted from Fig. 19 and was able to meet the desired rated speed with less noise and vibrations. The HTPMSM IPM type is then subjected to the load test in the hot chamber at an ambient temperature of 200°C by the variable frequency drive using the vector control strategy, and the obtained speed vs torque characteristics are depicted in Fig. 16. It is observed that the HTPMSM IPM type is delivering a constant torque until the base speed at an ambient temperature of 200°C, which validates the effectiveness of the proposed design as depicted from the simulation results shown in Fig. 11.

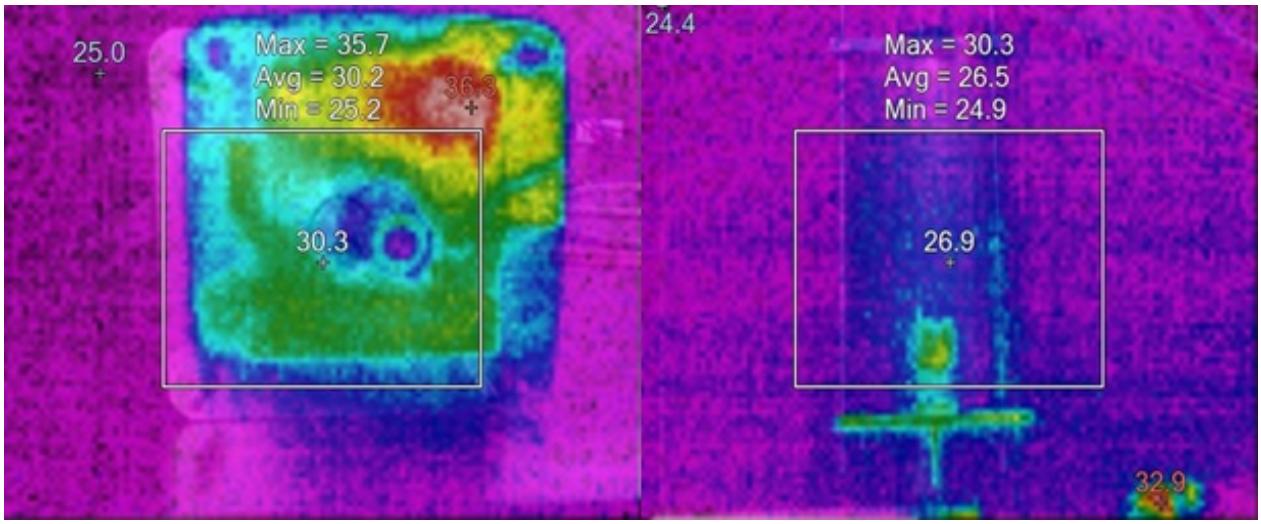

(a) View I (b) View II

Fig. 19. HTPMSM IPM type – temperature gradients

6. CONCLUSIONS

This research work addresses the design methodology for the high temperature PMSMs for robotic navigation applications. Two types of rotor configurations are designed and tested in real-time application. The rotor with the IPM configuration is able to sustain the required speed Vs torque characteristics of 2 Nm at the spinning speed of until 3 000 rpm for the defined volumetric and diametric constraints of 80×70 mm at the elevated temperature of 200°C. Also, the simulation-based FEM results of the HTPMSM IPM type rotor are validated with the designed prototype. The proposed design methodology shall be adaptable to the design of the miniature robots for various applications as they demand a high power and torque density ratio within the given frame size.

REFERENCES

[1] E. Sevinchan, I. Dincer, and H. Lang, "A review on thermal management methods for robots," *Appl. Therm. Eng.*, vol. 140, pp. 799–813, 2018, doi: 10.1016/j.applthermaleng.2018.04.132.

[2] Y. Li *et al.*, "Development and applications of rescue robots for explosion accidents in coal mines," *J. Field Robot.*, vol. 37, no. 3, pp. 466–489, 2020, doi: 10.1002/rob.21920.

[3] C. Buttay *et al.*, "State of the art of high temperature power electronics," *Mater. Sci. Eng.-B*, vol. 176, no. 4, pp. 283–288, 2011, doi: 10.1016/j.mseb.2010.10.003.

[4] X. Dong *et al.*, "Continuum robots collaborate for safe manipulation of high-temperature flame to enable repairs in challenging environments," *IEEE/ASME Trans. Mechatron.*, vol. 27, no. 5, pp. 4217–4220, 2022, doi: 10.1109/TMECH.2021.3138222.

[5] I. Josifovic, J. Popovic-Gerber, J.A. Ferreira, U. Drofenik, and E. Mengotti, "Thermal design of motor drives for high power density and long life in harsh environments," *IEEE Applied Power Electronics Conference and Exposition (APEC)*, 2015, pp. 2593–2600, doi: 10.1109/APEC.2015.7104717.

[6] A.M. EL-Refaie, "Electrical machines for harsh environments," *J. Eng.*, vol. 17, pp. 3489–3493, 2019, doi: 10.1049/joe.2018.8181.

[7] J.G. Lee, H.K. Yeo, H.K. Jung, T.K. Kim, and J.S. Ro, "Electromagnetic and thermal analysis and design of a novel-structured surface-mounted permanent magnet motor with high-power-density," *IET Electr. Power Appl.*, vol. 13, no. 4, pp. 472–478, 2019, doi: 10.1049/iet-epa.2018.5322.

[8] H.J. Yoon, Y.W. Nam, and K.S. Park, "A study on reliability improvement of BLDC motor for combat vehicle in high temperature environment," *J. Korean Soc. Manuf. Process Eng.*, vol. 17, no. 5, pp. 97–102, 2018. doi: 10.14775/ksmpe.2018.17.5.097.

[9] S. Li, B. Sarlioglu, S. Jurkovic, N.R. Patel, and P. Savagian, "Analysis of temperature effects on performance of interior permanent magnet machines for high variable temperature applications," *IEEE Trans. Ind. Appl.*, vol. 53, no. 5, pp. 4923–4933, 2017, doi: 10.1109/TIA.2017.2700473.

[10] H. Liu, L. Chow, and T. Wu, "November. Design of a permanent magnet motor with wide temperature range," *41st Annual Conference of the IEEE Industrial Electronics Society*, 2015, pp. 003816–003820, doi: 10.1109/IECON.2015.7392695.

[11] T.D. Kefalas, and A.G. Kladas, "Thermal investigation of permanent-magnet synchronous motor for aerospace applications," *IEEE Trans. Ind. Electron.*, vol. 61, no. 8, pp. 4404–4411, 2013, doi: 10.1109/TIE.2013.2278521.

[12] A.M. El-Refaie *et al.*, "Advanced high-power-density interior permanent magnet motor for traction applications," *IEEE Trans. Ind. Appl.*, vol. 50, no. 5, pp. 3235–3248, 2014, doi: 10.1109/TIA.2014.2305804.

[13] A. Wang, H. Li, and C.T. Liu, "On the material and temperature impacts of interior permanent magnet machine for electric vehicle applications," *IEEE Trans. Magn.*, vol. 44, no. 11, pp. 4329–4332, 2008, doi: 10.1109/TMAG.2008.2001527.

[14] M. Fasil, N. Mijatovic, B.B. Jensen and J. Holboll, "Performance variation of ferrite magnet PMBLDC motor with temperature," *IEEE Trans. Magn.*, vol. 51, no. 2, pp. 1–6, 2015, doi: 10.1109/TMAG.2015.2456854.

[15] Y. Kong, M. Lin, and L. Jia, "A novel high power density permanent-magnet synchronous machine with wide speed range," *IEEE Trans. Magn.*, vol. 56, no. 2, pp. 1–6, 2020, doi: 10.1109/ TMAG. 2019. 2947611.

[16] J.R. Hendershot and T.J.E Miller. *Design of brushless permanent-magnet machines*. Venice, FL, USA: Motor Design Books, 2010.

[17] M. Anand *et al.*, "An optimal selection of slot/pole combination and its influence on energy efficient PMSM for submersible water pumping applications," *Int. J. Ambient Energy*, vol. 44, no. 1, pp. 654–667, 2023, doi: 10.1080/01430750.2022.2140194.

[18] M. Sundaram, J. Chelladurai, M. Anand, P. Varunraj, S. Sharma, and M. El Haj Assad, "Performance Evaluation of Energy-Efficient Submersible Tubular Brushless Permanent Magnet Motor for Irrigation Application," *Arab. J. Sci. Eng.*, vol. 47, no. 11, pp. 14327–14341, 2022, doi: 10.1007/s13369-022-06744-2.

[19] H. Qiu, Y. Zhang, C. Yang, and R. Yi., "Influence of the number of turns on the performance of permanent magnet synchronous motor," *Bull. Pol. Acad. Sci. Tech. Sci.*, vol. 68, no. 3, pp. 429–436, 2020, doi: 10.24425/bpasts.2020.133375.